MODELING AND EMPIRICAL RESEARCH ON ENERGY PARTITIONING OF REGIONAL SEISMIC PHASES USED FOR EXPLOSION MONITORING

Mark D. Fisk[1], Thorne Lay[2], and Steven R. Taylor[3]

ATK Mission Research[1], University of California, Santa Cruz[2], and Rocky Mountain Geophysics, LLC[3]

Sponsored by National Nuclear Security Administration
Office of Nonproliferation Research and Development
Office of Defense Nuclear Nonproliferation

Contract Nos. DE-AC52-04NA25536[1], DE-FC52-04NA25537[2], and W-7405-ENG-36[3]

ABSTRACT

To gain theoretical insight into regional P/S discriminants and their frequency-dependent performance, source and attenuation models are used to predict spectra of regional seismic phases (Pn, Sn, and Lg) for nuclear explosions and selected earthquakes near the Lop Nor, Semipalatinsk (Balapan and Degelen Mountain), and Novaya Zemlya test sites in China and the former Soviet Union. A modified Brune (1970) model is used to predict P- and S-source terms for earthquakes. A Mueller/Murphy (1971) model is used for explosions, including a new conjecture that the S waves may be modeled by the same functional form as for P waves, but with corner frequency reduced by the ratio of near-source shear and compressional velocities. Results indicate that the frequency dependence of Pn/Sn and Pn/Lg discrimination performance at all of these hard-rock test sites is primarily due to differences in the corner frequencies of P and S waves for explosions, qualitatively consistent with observations by Xie and Patton (1999) for Pn/Lg at Lop Nor. P/S discrimination emerges at the explosion S-wave corner frequency and saturates at the P-wave corner frequency. In addition to explaining why P/S discriminants perform better at higher frequencies, these results suggest that their application should be restricted by a magnitude threshold and/or to frequencies near or above the explosion Pn corner frequency for a given source size, which can lead to practical monitoring limitations. Approximate scaling of the explosion S-wave corner frequency with elastic radius as $v_s(S)/R_e$ at all of these test sites suggests that major contributions to the phenomenon of S-wave generation from explosions may have a similar length scale as for P waves from explosions. The explicit physical mechanism of this near-source S generation is still being investigated.

Similar analyses are applied to nuclear explosions at the Nevada test site (NTS) and nearby earthquakes. Explicit information regarding geophysical working-point properties, depth of burial, and some announced yields for NTS explosions (Springer et al., 2002) is utilized for the modeling efforts. Geophysical effects on regional phases are examined for Yucca Flat, Pahute Mesa, and Rainier Mesa, as functions of media properties (type, density, velocities, gas porosity), source yield and depth, and for explosions above or below the water table.

Numerical simulation efforts are being initiated by UCSC to examine the partitioning and variability of regional seismic phases for various path and station effects, using the information (source models, etc.) obtained thus far by ATK/Mission Research. Using suites of explosion signals from each test site recorded at sets of stations, an attempt is made to isolate the near-source and near-receiver contributions to the variability of Pn arrivals. The basic strategy involves constraining the overall path effect by using closely spaced events recorded at a given station or closely spaced stations for a given source. Spectral and time domain measurements, corrected for event-averaged properties from multiple stations, are used to quantify the site or source region contributions. These measures will guide synthetic modeling with variable crustal properties beneath arrays of stations or arrays of sources.

OBJECTIVES

This is a three-year project to investigate energy partitioning of local and regional seismic phases to better understand mechanisms of P/S discriminants. We are analyzing Pn, Pg, Sn, and Lg spectra for underground nuclear explosions (UNEs) and earthquakes, and correcting for distance and source size, so that the variability of each type of phase may be assessed. We are comparing the corrected spectra to source models to explain the dependence of P/S discriminants on frequency, source size, and geophysical properties. Objectives are to quantify these aspects for explosions and earthquakes near the Lop Nor, Semipalatinsk, Novaya Zemlya, and Nevada test sites (LNTS, STS, NZTS, and NTS, respectively). We plan to interpret the variability of observations in terms of geophysical mechanisms by using complex elastic-screen simulations spanning relevant spectral content (0.1 to 10 Hz) for distances of at least 0 to 600 km and considering realistic models with multi-scale heterogeneity, rough Moho, topography, and other boundaries.

RESEARCH ACCOMPLISHED

The results of two studies are summarized below. The first focuses on spectral modeling of regional phases and P/S discriminants at the LNTS, STS, and NZTS in China and the former Soviet Union. Results for these hard-rock test sites were published by Fisk (2006). The second focuses on spectral analyses for explosions in tuff, rhyolite, and alluvium at NTS and for nearby earthquakes. In both studies, extended Mueller/Murphy (1971) (MM71) and Brune (1970) models are used to predict source terms of P and S waves for UNEs and earthquakes, respectively.

Spectral Modeling of Regional P/S Discriminants at Nuclear Test Sites in China and the Former Soviet Union

Fisk (2006) compared model and empirical spectra of Pn, Sn, and Lg for UNEs and earthquakes at LNTS in China, STS in Kazakhstan, and NZTS in the Arctic region of northern Russia. Distinctive aspects of this study are that (1) explicit models of P- and S-wave corner frequencies are provided in terms of near-source P and S velocities, and either stress drop and moment for earthquakes or elastic radius (which depends on yield and depth of burial) for explosions; and (2) the behavior of Pn/Sn and Pn/Lg is investigated at all of these test sites. Specifically new to this study, the explosion S waves are modeled using the same MM71 function as for P waves (as by Xie and Patton, 1999), but with Sn and Lg corner frequency reduced by the ratio of near-source S and P velocities: $v_s(S)/v_s(P)$. This is analogous to the extension of the Brune model for earthquake P and S waves, with the corner frequencies depending on the P and S velocities (as by Taylor et al., 2002). The same MM71 and Brune models are used at all hard-rock test sites.

Figure 1 shows locations of explosions, earthquakes, and digital seismic stations within 2000 km of LNTS and STS (except for TLY and ULN). Many STS UNEs up to 1989 were recorded digitally by BRV (Borovoye, Kazakhstan) and WMQ (Urumqi, China). More recent events, including LNTS UNEs since mid 1994, were recorded digitally by up to 19 regional stations in Kazakhstan, Kyrgyzstan, Pakistan, Russia, Mongolia, and China. Instrument-corrected spectra of Pn, Pg, Sn, and/or Lg were processed for 9 UNEs since 1992 at LNTS and 156 nearby earthquakes. To model the UNEs, yields (W) were estimated using mb = 0.75 log W + 4.4, and scaled depth of burial was assumed. Earthquakes on 1999/01/27 (mb 3.95) and 1999/01/30 (mb 5.40) are particularly useful because they were at LNTS. Spectra were also processed for 51 UNEs (47 by BRV and 28 by WMQ) at STS between 1983 and 1989, and 87 earthquakes (mb 3.2 to 5.5) in the Reviewed Event Bulletin (REB) from 1995 to 2002. An mb 3.8 earthquake (labeled by *jdate* 1996086 in Figure 1) was closest to STS and was recorded by 17 regional stations, including BRVK and WMQ. A yield of 115 kt and depth of 600 m (Sykes and Ekström, 1989; Murphy and Barker, 2001) were used to compute model results for the Soviet JVE on 1988/09/14. For all other Balapan explosions, yields were estimated using mb = 0.75 log W + 4.45 (Murphy and Barker, 2001), and assuming scaled depth of $h = 122\ W^{1/3}$. Murphy (pers. comm., 2005) provided yields and depths from the Institute for the Dynamics of the Geospheres (IDG) in Moscow, Russia for 23 Degelen UNEs between 1964 and 1989, although it is not clear how the IDG determined the values or what the uncertainties are.

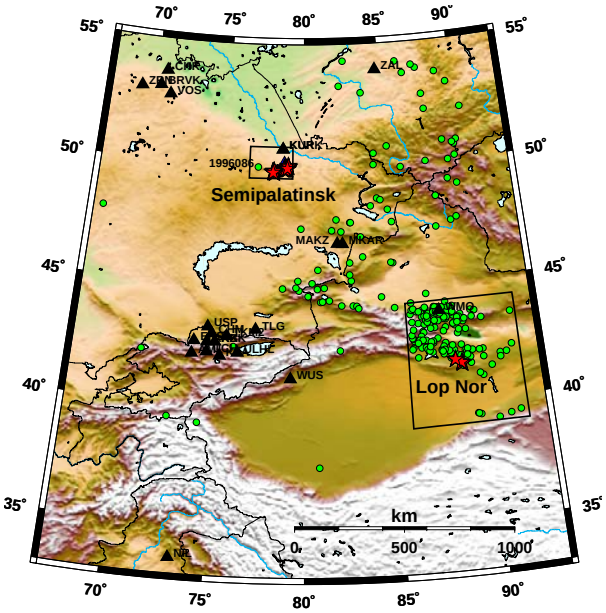

Figure 1. Locations of nuclear explosions (stars), earthquakes (circles), and seismic stations (triangles) within regional distances of LNTS and STS.

Figure 2 shows events at or near NZTS, recorded by NORSAR, NORES, ARCES, and/or KEV. Locations and magnitudes were compiled from Ringdal (1997), NORSAR (1999), and the ISC. ARCES, NORES, and KEV recorded only 3 to 6 NZTS UNEs from 1982 to 1990, with a limited mb range of 5.5 to 5.8, which do not allow study of source scaling effects. From 1976 to 1990 NORSAR recorded 17 UNEs (mb 3.8 to 6.0) at the test site near Matochkin Shar. Most NORSAR elements were clipped for most of these UNEs. The NAO01 element includes some short-period recordings at high gain (sz), and many at low gain (slz; gain reduced by 30 dB), that were not clipped. Thus, NAO01 data are the most useful for this P/S study at NZTS. Since NORSAR is over 20 degrees away, adequate S-wave signal-to-noise ratio (SNR) for these events is limited to below about 3 to 4 Hz. Based on analysis by Murphy and Barker (2001), the same mb:yield relation is used for NZTS and STS. It is also interesting to consider aftershocks – perhaps the only ground-truth earthquakes in the vicinity – that were triggered by megaton UNEs in 1973 and 1974 (e.g., Israelsson et al., 1974), including the largest UNE (3.5 mt) at the southern (Krasino) area on 1973/10/27. Three of the larger aftershocks (mb 4.5–4.6) and the 1986/08/01 Kara Sea event, identified as an earthquake by Marshall et al. (1989), are considered.

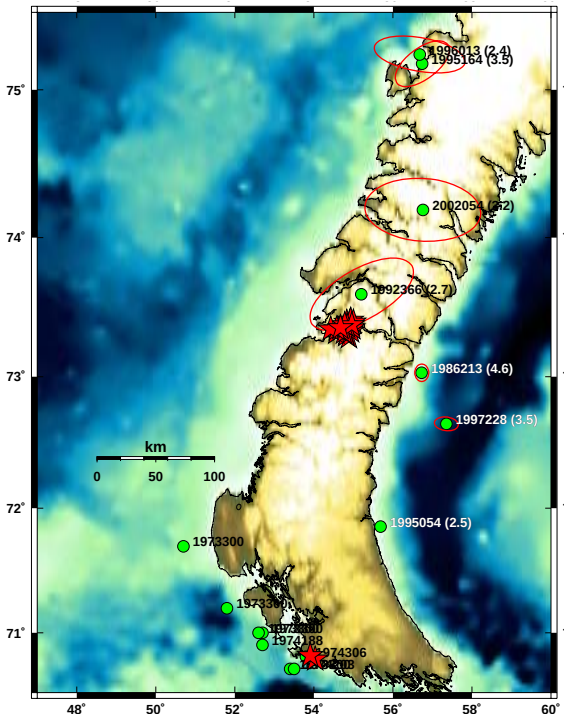

Figure 2. Locations of UNEs (stars) and other events (circles) recorded by KEV, ARCES, NORES, and/or NORSAR. Circles at the southern end of NZ represent aftershocks, induced by megaton-range UNEs. Julian dates, mb values (in parentheses), and location error ellipses are shown for selected events.

Spectra of regional seismic phases were modeled for the Lop Nor, Degelen, Balapan, and Novaya Zemlya test sites, using extended Brune and MM71 source models, and attenuation and station corrections that were estimated for the various paths and stations. (See Fisk, 2006, for details.) Figure 3, for example, compares instrument-corrected Pn, Sn, and Lg spectra to model predictions at MAK (top) for the 1999/01/30 earthquake (left) and the 1996/06/08 UNE at LNTS (right) and at WMQ (bottom) for the 1996/03/26 earthquake (left) and the 1988/09/14 JVE at STS (right). The gray curves in each plot show the model predictions. Since the station terms were computed using the nearby earthquake data, the model comparisons to the earthquake spectra are expected to agree quite well, at least over the frequency range for which the spectra have adequate SNR. The model and empirical spectra for the explosions also compare quite well and provide independent indication that the attenuation and station corrections are reasonable.

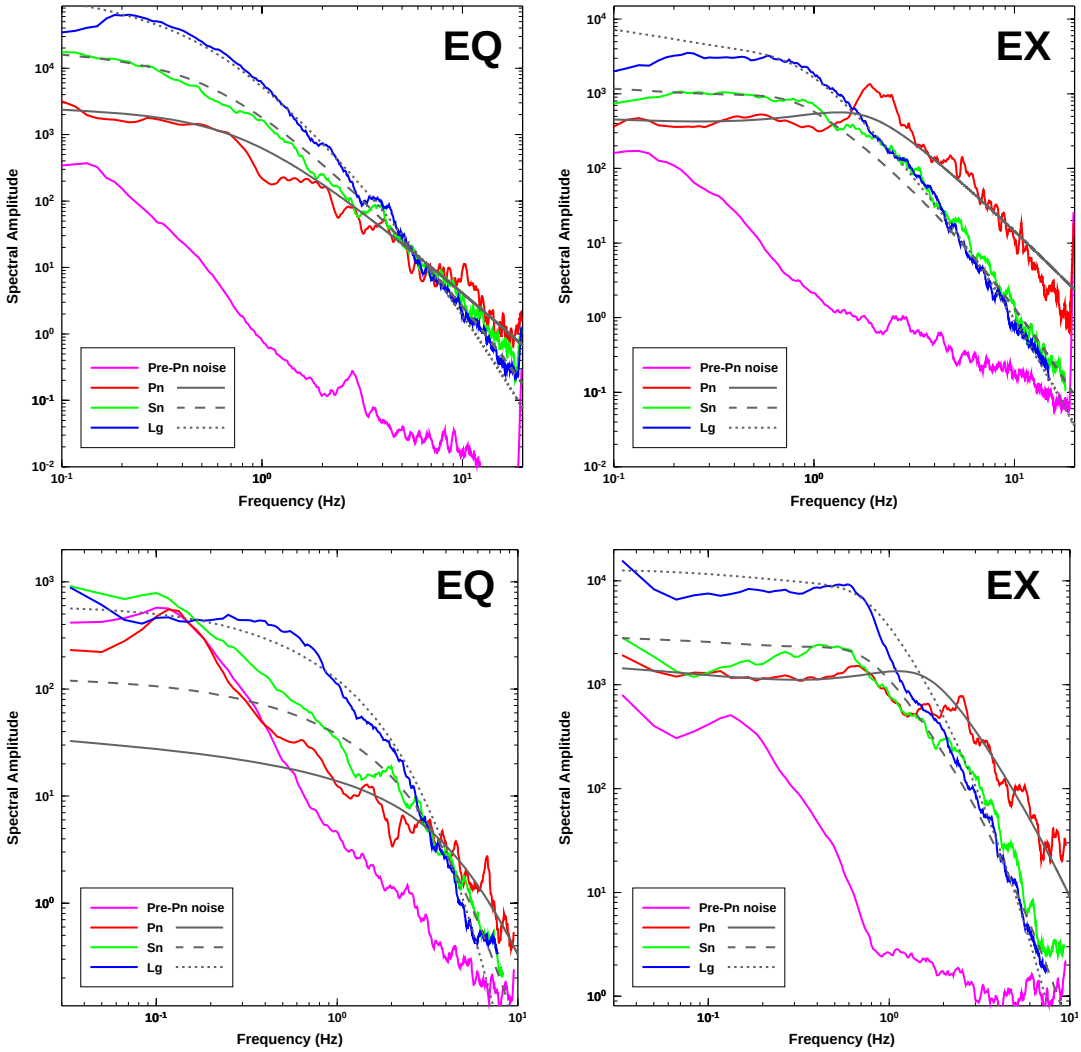

Figure 3. Instrument-corrected Pn, Sn, and Lg spectra at MAK (top) for the 1999/01/30 earthquake (left) and 1996/06/08 UNE (right) and at WMQ (bottom) for a 1996/03/26 earthquake (left) and 1988/09/14 JVE (right). Corresponding model predictions, including attenuation and station terms, are also shown (gray curves).

Figure 4 shows Pn/Sn spectral ratios for 9 LNTS UNEs (magenta curves), the two 1996 UNEs (red curves), and two 1999 earthquakes (green curves), using preliminary distance and station corrections, and then network averaging. (A plot of the Pn/Lg spectral ratios is very similar.) Model results are shown for the 1996 UNEs and 1999 earthquakes (black and gray curves, respectively). They seem to adequately fit the data and indicate that the frequency dependence of P/S discrimination performance is mainly due to different corner frequencies of P and S waves for explosions. Note that, using either the modified Brune or MM71 models, the ratio of high-frequency to low-frequency asymptotic limits of P/S spectral ratios for earthquakes and explosions is given by the ratio of P to S corner frequencies squared. Thus, frequency-dependent discrimination performance is governed by the ratio of the corner frequencies squared and dominated by the event type for which the P and S corner frequencies differ the most. The separation of P/S ratios for earthquakes and explosions is mainly due to the ratio of S and P velocities in the extended Brune model, and a constant k of explosion S-wave coupling (introduced by Fisk, 2006), that was empirically fit for each test site.

Figure 5 shows Pn/Lg spectral ratios at WMQ for 18 UNEs at Balapan, averaged in three mb bins (13 at mb 5.9-6.2, 3 at mb 5.4-5.8, and 2 at mb 4.9-5.1), and for the 1996/03/26 earthquake using WMQ data only (cyan) and averaging over 17 stations (green). Corresponding model results are depicted by the black and gray curves. Figure 6 shows Pn/

Lg spectral ratios at WMQ, corrected for attenuation and site terms, for 6 Degelen UNEs (red curves). The gray curve in each plot is the Brune model result for the earthquake. The solid black curves are the MM71 results for each UNE, using the yields and depths provided by the IDG. The dashed curves are model results using the yields provided and scaled depth of burial. Above about 0.3 Hz, the model results in Figures 5 and 6 seem to suitably predict the empirical Pn/Lg spectral ratios, considering that only one station is used. They do not compare as well below about 0.3 Hz because the Pn attenuation and station corrections are poorly constrained at lower frequencies (cf. bottom left plot of Figure 3) and Pn signals are biased higher by noise. The extended MM71 model, with different corner frequencies for P and S waves, seems to adequately predict Pn/Lg discrimination at STS, as at LNTS.

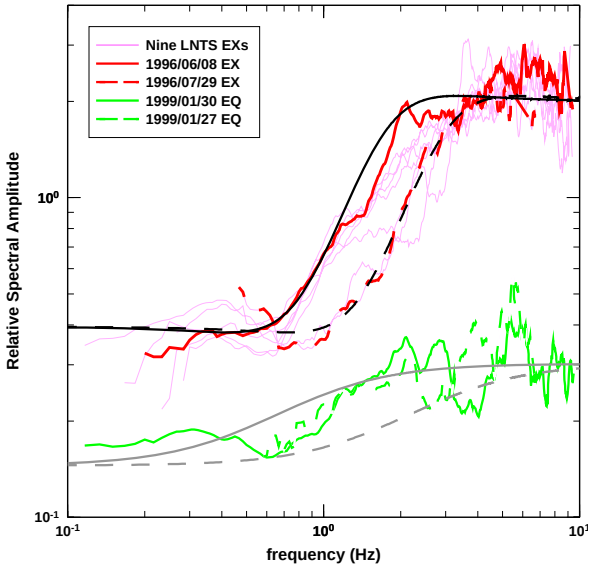

Figure 4. Network-averaged Pn/Sn spectral ratios, corrected for attenuation and station effects, for nine LNTS explosions and two January 1999 earthquakes. Model predictions are shown for the 1996 explosions and the 1999 earthquakes (black and gray curves).

Last, P/S spectral ratios were examined for events at NZTS. Ringdal et al. (1998) noted that P/S ratios in the 1–3 Hz band appear to depend on magnitude for these UNEs, with the smaller ones having lower P/S ratios. Figure 7 shows P/S spectral ratios (for 17 NZTS UNEs), corrected for attenuation and site effects, and averaged in two mb bins (red curves), and for the earthquakes (green and cyan curves). Model predictions are shown for the UNEs (black curves) and an mb 4.6 earthquake (gray curve). The explosion P and S corner frequencies were both increased by 20%, for shale/sandstone at NZTS (Khalturin et al., 2005), compared to granite at LNTS and STS. However, the P and S corner frequencies for NZTS UNEs were still scaled as the ratio of the P and S velocities. Hence, these model results indicate the same explanation of frequency-dependent P/S discrimination performance and dependence on source size, in terms of the relative explosion P and S corner frequencies.

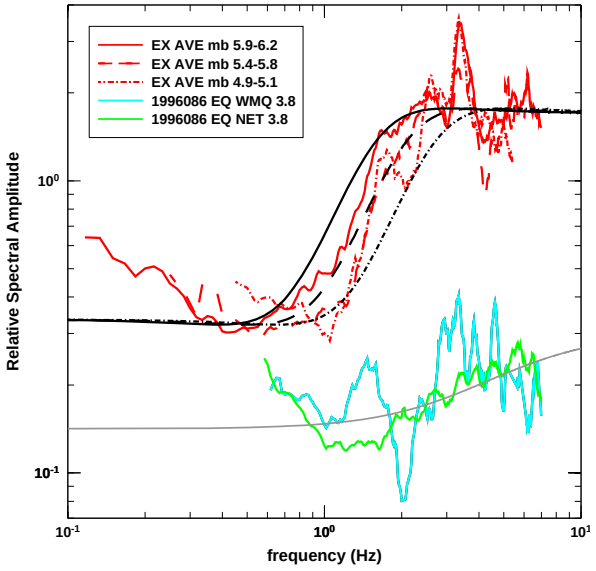

Figure 5. Model and empirical Pn/Lg spectral ratios at WMQ for 18 Balapan UNEs, averaged in three mb bins, and the 1996/03/26 earthquake.

Analysis of Regional P/Lg Discriminants at NTS

We processed Pn, Pg, and Lg spectra for 69 explosions and 38 earthquakes at or near NTS, that were provided by Dr. Walter of LLNL. Figure 8 shows locations of the events. We corrected the spectra for distance and station effects, based on parameters from Walter and Taylor (2002). We have been comparing spectral scaling for various phases and spectral ratios (Pg/Lg and Pn/Lg) to model calculations, using extended Brune and MM71 models for P and S phases, with appropriate geophysical parameters for NTS. For this modeling work, we have utilized explicit information regarding working-point (WP) material properties, depths, and some announced yields for NTS UNEs (Springer et al., 2002).

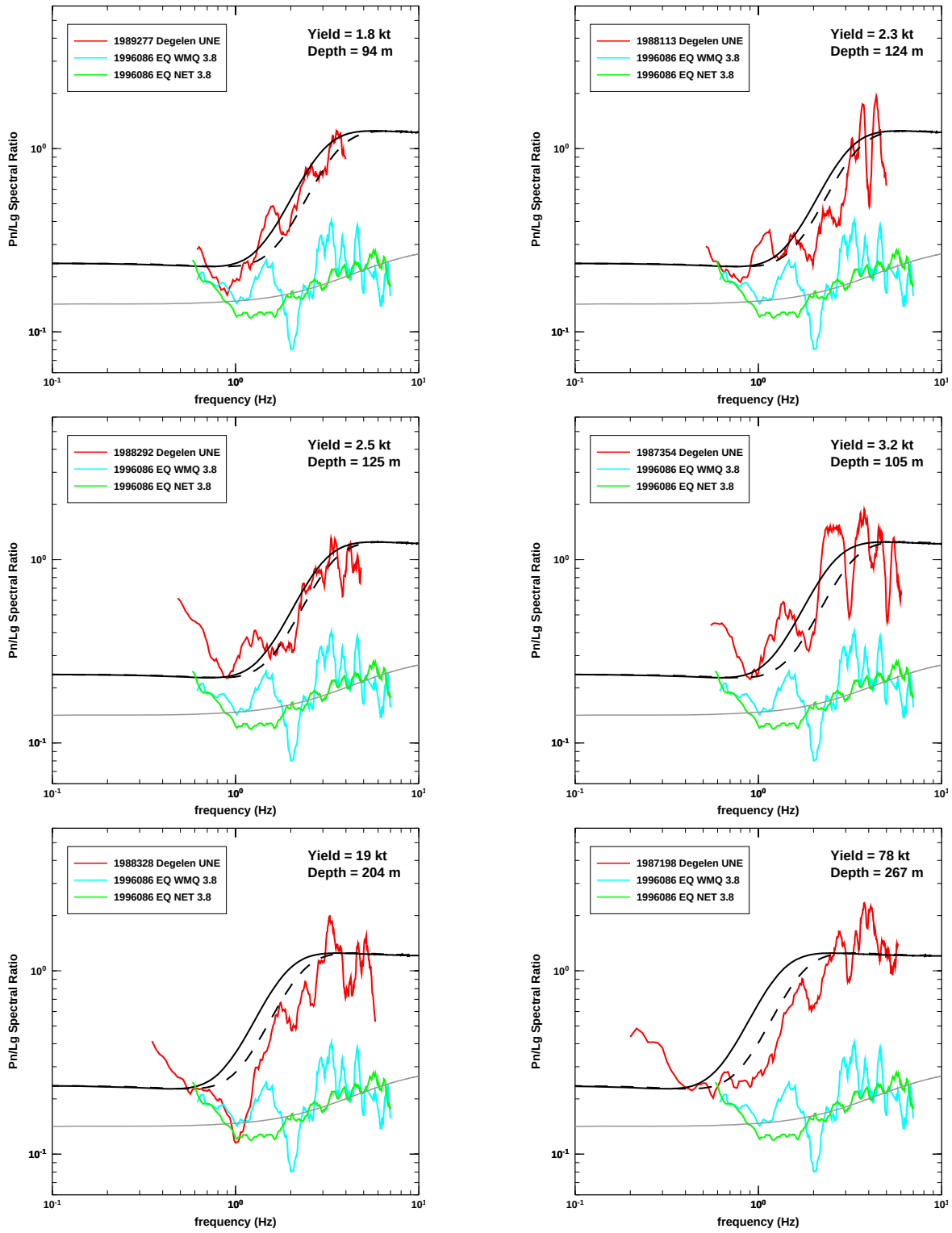

Figure 6. Comparison of empirical and model Pn/Lg spectral ratios at WMQ for 6 Degelen explosions and the 1996/03/26 earthquake. The model results were computed using the yields reported by the IDG and either the depths reported (solid black) or scaled depths (dashed black).

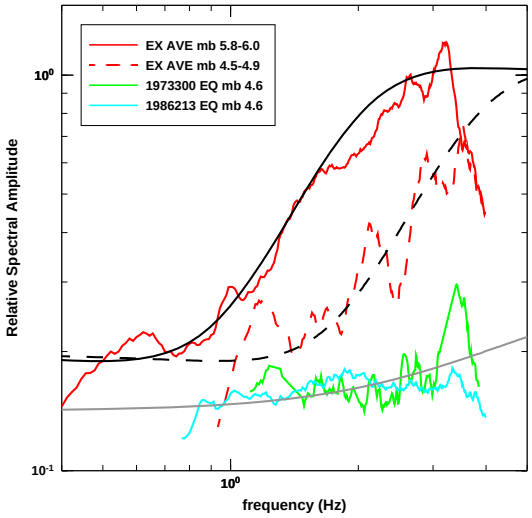

Figure 7. Corrected P/S spectral ratios at NAO01 for 17 NZTS UNEs, averaged in two mb bins, the 1986 Kara Sea event, and an aftershock in 1973. The black and gray curves depict corresponding model results.

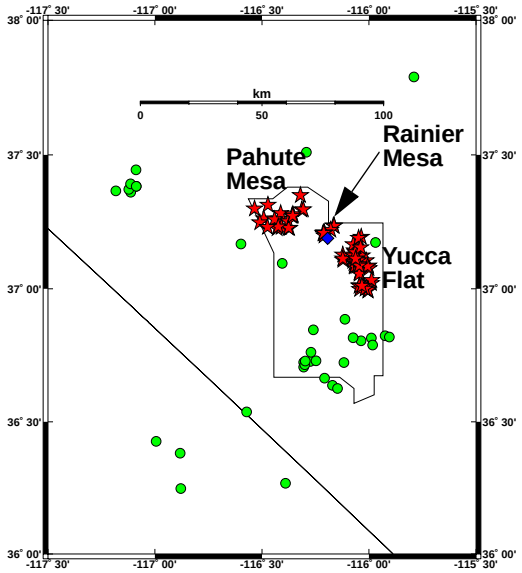

Figure 8. Locations of earthquakes (circles), UNEs (stars), and the NPE (diamond) at NTS.

Among other investigations, we examined whether NTS UNEs exhibit similar relative scaling of P and S corner frequencies as UNEs at the other (hard rock) test sites. To do this, we fit the corner frequencies of a generic MM71 model to the corrected Pn, Pg, and Lg spectra that minimizes the RMS residuals. Figure 9 shows examples of Pn, Pg, and Lg spectra, corrected for instrument response, distance, and site effects, and averaged over ELK, KNB, LAC, and MNV, for two explosions, one at Rainier Mesa (RM) and one at Yucca Flat (YF). Also shown are the fits of MM71 to these corrected spectra.

Figure 10 shows the estimated Pn, Pg, and Lg corner frequencies versus yield for UNEs at RM (top) and at YF (bottom) with gas porosities less than 10%. Also shown are theoretical (MM71) P-wave corner frequencies (gray circles), using the depth and WP material properties for each UNE from Springer et al. (2002). Since each set of these shots were in media with similar properties (e.g., densities of 1.88 to 1.97 g/cm^3 for RM) and at fairly similar depths, the mean properties and depths for each set were used to compute the gray lines, which scale as $W^{-1/3}$. The dashed gray lines are simply shifted lower. The Pn, Pg, and Lg corner frequencies appear to all have similar trends with yield, and fairly consistent with the theoretical predictions. Pg shows the most deviation from the theoretical. Lg shows the best agreement with the theoretical MM71 corner frequency scaling.

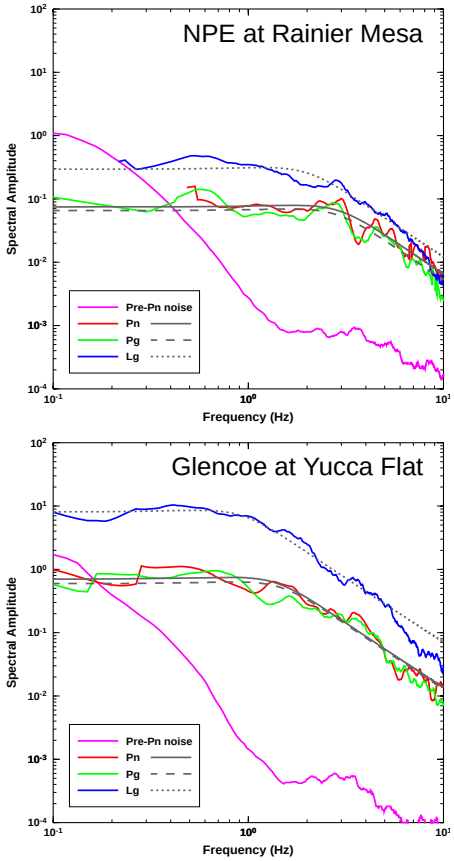

Figure 9. Comparison of model fits to corrected and network-averaged Pn, Pg, and Lg spectra for the Non-Proliferation Experiment (NPE) and Glencoe.

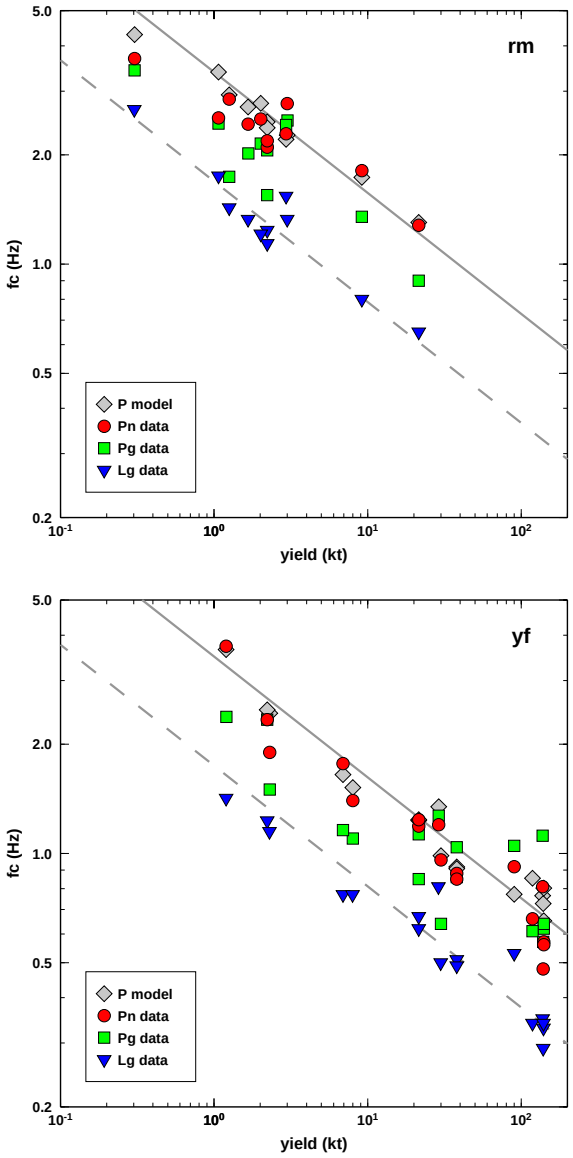

Figure 10. Estimated corner frequencies of Pn, Pg, and Lg versus yield for UNEs at RM (top) and below the water table at YF (bottom). Gray lines are model predictions using the mean material properties and depths for each respective set. Gray dots are MM71 P-wave corner frequencies using the explicit material properties and depths for each explosion.

Since material properties and depths for UNEs at Pahute Mesa have greater variations, we plot the log difference of empirical corner frequencies, relative to MM71 model results for P waves, versus yield (Figure 11). The lack of trends in the residuals suggests good agreement between the empirical and MM71 corner frequencies, as well as similar corner frequency scaling for Pg and Lg. We also examined UNEs above the water table at YF. These data exhibit similar behavior, although there is much more scatter, presumably due to greater variations in the material type (tuff and alluvium) and gas porosity. Despite greater scatter in the data at NTS than at hard-rock test sites, it appears that explosion Lg corner frequencies exhibit similar scaling as P waves, as was observed at LNTS, STS, and NZTS.

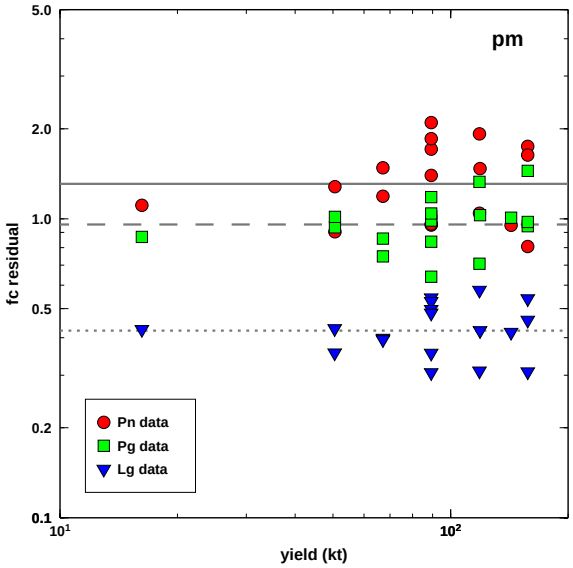

Figure 11. Residuals of model and empirical Pn, Pg, and Lg log corner frequencies versus yield for UNEs at Pahute Mesa. Model results were computed using MM71 for P waves and the depths and WP material properties for each UNE from Springer et al. (2002).

CONCLUSIONS AND RECOMMENDATIONS

Extended MM71 and Brune models were first used to predict source spectra of P and S waves for UNEs and earthquakes near LNTS, STS (Balapan and Degelen), and NZTS. Key results from this study (Fisk, 2006) are as follows. First, frequency dependence of regional P/S discriminants appears to be mainly due to differences in P and S corner frequencies for explosions. The modified Brune and MM71 models used here both predict that the ratio of high-frequency to low-frequency asymptotes of P/S spectral ratios equals the ratio of the P to S corner frequencies squared. Using geophysical parameters from Taylor et al. (2002) and Stevens and Day (1985), model predictions of this ratio are about 2 for the earthquakes and about 5 for explosions. Note that the same relative corner frequency scaling was used for explosion P and S waves throughout this study. Thus, the model provides the same interpretation of frequency-dependent Pn/Sn

and Pn/Lg discrimination at all of the hard-rock test sites examined here. Namely, P/S discrimination begins to emerge predominantly at the explosion S-wave corner frequency and saturates at the explosion P-wave corner frequency. This theoretical result is in agreement with empirical experience obtained over several decades. Also, the dependence of P/S spectral ratios on explosion size at all of these test sites (i.e., lower P/S ratios for smaller explosions at frequencies between the P and S corner frequencies) is qualitatively consistent with observations by Xie and Patton (1999) for LNTS and Ringdal et al. (1998) for NZTS, now with a consistent model-based explanation. An important caveat regarding these results is that limited GT information is available on explosive yield, depth of burial, and other emplacement conditions. Some details of the quantitative results may change if more accurate or explicit information becomes available. However, the conjecture of the relative explosion P and S corner frequencies, which seems to explain the main frequency dependence of P/S discrimination, does not depend on the explicit parameters (i.e., the ratio was the same for all explosions at the hard-rock test sites).

Second, in addition to explaining why P/S discriminants typically perform better at higher frequencies, these results suggest that their application should be restricted by a magnitude threshold and/or to frequencies near or above the explosion Pn corner frequency for a given source size. This can lead to practical monitoring limitations, depending on the size of the explosion, the proximity of regional stations, and SNR, which must be evaluated on a case-specific basis. For example, Figure 6 illustrates that useful discrimination is achieved for explosions down to ~1 kt or perhaps lower at STS, using WMQ recordings at distances of about 1000 km. The performance will degrade for smaller explosions or ones recorded by farther or noisier stations, as SNR degrades near or above the Pn corner frequency. However, a compensating factor is that smaller explosions have more relative high-frequency content in their seismic signals, so (as Figure 6 also indicates) the performance does not degrade as rapidly with yield as might be expected.

Third, the apparent scaling of the explosion S-wave corner frequency with the elastic radius as $\omega_0(S) = v_s(S)/R_e$ at all of the Lop Nor, Degelen, Balapan, and Novaya Zemlya test sites is either an inexplicable coincidence or it suggests that explosion S waves are generated predominantly at a similar length scale as explosion P waves. One would expect that explosion P and S waves would have the same corner frequencies if the S waves are from linear P-to-S conversion, such as at the free surface near the source or by heterogeneities along the path. Alternatively, one would not expect to find any consistent relationship between explosion P and S corner frequencies if the S waves are generated by nonlinear spall effects that can vary greatly with emplacement conditions (e.g., overburden and vertical borehole versus tunnel). While the explicit physical mechanism for near-source S-wave generation is not yet understood, the implications are important regarding where and perhaps how S waves are generated by explosions.

Preliminary results for NTS require further review, but seem to indicate that Lg corner frequencies scale approximately as a constant factor of P corner frequency scaling, as at other nuclear test sites on hard rock. If these results are correct, then they corroborate a very important effect, i.e., that explosion S waves are being generated predominantly near the source. We have also been investigating variations in overall coupling strength of various seismic phases, which appear to be greater than at hard-rock test sites, and effects of spectral modulations on P/Lg discriminants at NTS. Numerical simulations are planned to investigate various near-source and scattering effects that might explain these variations.

We plan to continue our modeling and analysis efforts for NTS, including examination of geophysical effects for Yucca Flat, Pahute Mesa, and Rainier Mesa, based on the type of media, density, velocities, gas porosity, yield, depth of burial, and for UNEs above or below the water table. More work is needed to examine the behavior of P/S discriminants for other geological region types and many more events, but a consistent model-based understanding of P/S discrimination seems to be emerging. Such understanding could potentially be used to predict discrimination performance, on average, for regions with sufficient information. Considerably more work is required to understand regional phase variability due to a multitude of path (scattering) and station effects. More theoretical and numerical-simulation work is also needed to understand the explicit physical mechanism of near-source S generation.

ACKNOWLEDGMENTS

We are grateful to Gary McCartor, Howard Patton, and Jiakang Xie for many useful discussions, and to Scott Phillips, George Randall, and Bill Walter for providing seismic data, moments, stress drop values, and attenuation parameters.

REFERENCES

Brune, J. N. (1970). Tectonic stress and the spectra of seismic shear waves from earthquakes, *J. Geophys. Res.*, 75: 4997–5009.

Fisk, M. D. (2006). Source spectral modeling of regional P/S discriminants at nuclear test sites in China and the former Soviet Union, in press, *Bull. Seism. Soc. Am.*

Israelsson, H., R. Shunga, O. Dahlman (1974). Aftershocks caused by the Novaya Zemlya explosion on October 27, 1973, *Nature*, 247: 450–452.

Khalturin, V. I., T. G. Rautian, P. G. Richards, and W. S. Leith (2005). A review of nuclear testing by the Soviet Union at Novaya Zemlya, 1955-1990, *Science and Global Security*, 13, 1–42.

Marshall, P. D., R. C. Stewart, and R. C. Lilwall (1989). The seismic disturbance on 1986 August 1 near Novaya Zemlya: a source of concern?, *Geophysical Journal* 98: 565–573.

Mueller, C. S. and J. R. Murphy (1971). Seismic characteristics of underground nuclear detonations Part I: seismic spectrum scaling, *Bull. Seism. Soc. Am.* 61: 1675–1692.

Murphy, J. R. and B. W. Barker (2001). Application of network-averaged teleseismic P-wave spectra to seismic yield estimation of underground nuclear explosions, *Pure and Appl. Geophys., Special Edition on Monitoring the Comprehensive Nuclear-Test-Ban Treaty: Source Processes and Explosion Yield Estimation*, 158: 2123–2171.

NORSAR (1999). Novaya Zemlya Explosions 1971–1990 Research and Development Database, Seismic records from the large aperture NORSAR array in CSS3.0 format, June, 1999.

Ringdal, F. (1997). Study of low-magnitude seismic events near the Novaya Zemlya nuclear test site, *Bull. Seism. Soc. Am.*, 87: 1563–1575.

Ringdal, F., E. Kremenetskaya, V. Asming, T. Kvaerna, J. Fyen, and J. Schweitzer (1998). Seismic Monitoring of the Barents/Kara Sea Region, in *Proceedings of the 20th Annual Seismic Research Symposium on Monitoring a Comprehensive Test Ban Treaty*, pp. 21–23.

Springer, D. L., G. A. Pawloski, J. L. Ricca, R. F. Rohrer, and D. K. Smith (2002). Seismic source summary for all U.S. below-surface nuclear explosions, *Bull. Seism. Soc. Am.* 92: 1806–1840.

Stevens, J. L. and S. M. Day (1985). The physical basis of the mb:Ms and variable frequency magnitude methods for earthquake/explosion discrimination, *J. Geophys. Res.* 90: 3009–3020.

Sykes, L. R. and G. Ekström (1989). Comparison of seismic and hydrodynamic yield determinations for the Soviet joint verification experiment of 1988, *Proc. Natl. Acad. Sci.* 86: 3456–3460.

Taylor, S. R., A. A. Velasco, H. E. Hartse, W. S. Phillips, W. R. Walter, and A. J. Rodgers (2002). Amplitude corrections for regional seismic discriminants, *Pure and Appl. Geophys., Special Edition on Monitoring the Comprehensive Nuclear-Test-Ban Treaty: Seismic Event Discrimination and Identification*, 159: 623-650.

Walter, W. R. and S. R. Taylor (2002). A Revised Magnitude and Distance Amplitude Correction (MDAC2) Procedure for Regional Seismic Discriminants: Theory and Testing at NTS, *UCRL-ID-146882, LA-UR-02-1008*.

Xie, J. and H. J. Patton (1999). Regional phase excitation and propagation in the Lop Nor region of central Asia and implications for P/Lg discriminants, *J. Geophys. Res.* 104: 941–954.